Available online at www.sciencedirect.com

SciVerse ScienceDirect

Magnetic Resonance Imaging 30 (2012) 934–943

MAGNETIC RESONANCE IMAGING

The effect of temporal sampling on quantitative pharmacokinetic and three-time-point analysis of breast DCE-MRI

Jacob U. Fluckiger, Matthias C. Schabel, Edward V.R. DiBella*

Department of Radiology, Utah Center for Advanced Imaging Research, University of Utah, Salt Lake City, UT 84108, USA

Received 3 May 2011; revised 15 February 2012; accepted 17 February 2012

Abstract

The effects of temporal sampling on the previously published three-time-point (3TP) method are compared with those of a Tofts–Kety model using an arterial input function from the alternating minimization with model (AMM) method. Computer simulations are done to estimate the expected error in both the 3TP and Tofts–Kety models as a function of the temporal sampling rate of the data. The error in the 3TP model parameters remained essentially constant with respect to temporal sampling. The Tofts–Kety model showed a linear increase in parameter error with respect to temporal sampling. Both analysis methods were also applied to 87 clinically acquired breast scans. These scans were downsampled in time by a factor of 2 and 4, and the methods were reapplied. The spatial resolution was held constant throughout this study. At temporal resolutions less than 19.4 s, the Tofts–Kety model outperformed the 3TP model using receiver operating characteristic curve analysis (area under the ROC curve [AUC] of 0.94 compared to 0.91). As the temporal sampling rate decreased, the 3TP model outperformed the Tofts–Kety model (AUC of 0.89 versus 0.85). When the temporal sampling rate of the data was less than 20 s, the Tofts–Kety model with the AMM method had lower parameter error than the 3TP method.

Keywords: Pharmacokinetics; Breast cancer imaging; Contrast-enhanced MRI; Temporal sampling

1. Introduction

Dynamic contrast-enhanced magnetic resonance imaging (DCE-MRI) is a physiological imaging tool that has been used to complement established diagnostic methods in evaluating breast lesions. DCE-MRI has been shown to provide high sensitivity and moderate specificity in detecting breast cancer (see reviews in Refs. [1,2]). In addition, changes in tumor volume as measured with DCE-MRI have been shown to correlate well with response to chemotherapy [3,4].

Many methods for analyzing DCE-MRI data have been proposed. These methods include qualitative assessment of morphological features, semiquantitative parameters such as signal enhancement, contrast wash-in and wash-out rates, and quantitative pharmacokinetic modeling (see references in Ref. [2]). In addition, more recent analysis techniques such as fuzzy c-means clustering [5], principal component analysis [6] and textural kinetics [7] have been proposed for automatic identification of breast lesions. Selecting an optimal analysis method remains an open question. This work focuses on two more commonly used techniques for classifying lesions with DCE-MRI: the semiquantitative three-time-point (3TP) method [3,6,8–14] and the quantitative extended Tofts–Kety (ETK) two-compartment model [15–18].

One issue for analyses using the ETK model with breast DCE-MRI involves the accurate acquisition of the arterial input function (AIF). Automatic detection techniques have been proposed for selecting the AIF from the breast DCE-MRI data [19]. However, due to the relatively small size of the axillary and internal mammary arteries, the measurements may suffer from partial volume effects [20]. Direct measurement of the AIF from the cardiac blood pool is another possibility but requires use of an extended field of view, potentially compromising spatial and/or temporal resolution. Furthermore, there is growing evidence that tumor blood supply may be substantially different from that of surrounding normal tissues [21,22]. Population-average input functions have also been proposed [18,23], though these are necessarily limited in their response to interpatient

* Corresponding author. Tel.: +1 801 585 5543; fax: +1 801 585 3592.
E-mail address: ed@ucair.med.utah.edu (E.V.R. DiBella).

0730-725X/$ – see front matter © 2012 Elsevier Inc. All rights reserved.
doi:10.1016/j.mri.2012.02.011

variation. Other work has been performed using reference regions to estimate model parameters [24–26], which remove the need for an AIF. This work employs a blind estimation method for determining a parameterized AIF directly from measured tissue enhancement curves [22,27,28]. The blind AIF estimation can be done at an arbitrarily high sampling rate, alleviating some of the constraints inherent in quantitative modeling.

The question of whether to use a semiquantitative model, like the 3TP method, or a quantitative model, such as the ETK method, is highly influenced by the temporal sampling rate of images being acquired. Images with high spatial resolution are well suited for qualitative assessment of areas with contrast uptake and washout and are often used to segment breast lesions into fine heterogeneous structures. Quantitative analyses, on the other hand, are generally more sensitive to temporal sampling rate than the semiquantitative methods. These quantitative methods fit mathematical models to measured data, and rapid sampling of the data is required for good model fidelity. As mentioned above, quantification of tissue kinetics with the ETK model requires an AIF. In general, the AIF varies more rapidly in time than tissue curves, and the limits on temporal sampling are driven by the AIF. The rate at which the AIF and tissue curves should be sampled is an area of active research and depends on the particular model implementation chosen as well as the tissue physiology [17,29–31]. Recent work by both Planey et al. and Heisen et al. has focused mainly on reference region techniques using the so-called 'standard' Tofts model, which does not explicitly account for the plasma volume fraction within the tissue [17,30,31]. These methods estimate the error in the model parameters as a function of the temporal sampling rate of the DCE-MRI data. In comparison, previous work by Henderson et al. [29] focuses on simulations to show the effects of the temporal sampling rate with the plasma volume fraction included in the model, as well as with a more conventionally sampled AIF.

This work aims to compare the quantitative ETK analysis method to the more commonly used 3TP semiquantitative analysis at different temporal sampling rates. The alternating minimization with model (AMM) algorithm is used to estimate the AIF for analysis with the ETK method [27]. Computer simulations are used to investigate the ability of the ETK model to accurately return pharmacokinetic parameters at various temporal resolutions. The blind estimation implementations are done at 1-s temporal resolution, consistent with the recommendations of Henderson et al. [29]. These simulations also test the ability of the 3TP model to accurately return semiquantitative parameters at various temporal sampling rates. Both the ETK and 3TP models are applied to previously acquired breast DCE-MRI data in which pathology results are known. The ability of the respective methods to distinguish benign and malignant breast lesions, as measured by the area under the receiver operator characteristic (ROC) curve (AUC), are determined as a function of the temporal sampling rate of the acquired data.

2. Methods

2.1. 3TP method

The 3TP method [8,11,13,14], which is based on the standard Tofts–Kety model with no volume plasma fraction, is a parametric description of individual tissue curves that assigns each voxel in the image a color (red, green or blue) and color intensity. Three samples or time points from each time curve are considered. The time points used here are one time point precontrast, one 2 min following contrast injection and one 6 min following contrast injection. The intensity of the color of each voxel is directly related to the relative change in signal intensity between the first and second time points, and reflects the rate at which the contrast agent is initially taken up into the voxel. The color of each voxel is related to the relative change in signal intensity between the second and third time points. Voxels with at least a 10% increase in signal enhancement are colored blue, voxels whose signal enhancement changes by less than 10% are green, and voxels with a 10% or greater decrease in signal enhancement are colored red. A calibration map is used to ensure consistency across images [11,14]. 3TP analysis is typically done with data acquired with a 1–2-min temporal sampling rate [8,12,13].

2.2. ETK model

The ETK model is a compartmental model that describes the tissues being imaged as a mixture of two compartments (one blood, one tissue) into and out of which the contrast agent can flow. Mathematically, the ETK model is given as:

$$C_t(t) = K^{trans} C_p(t) \otimes e^{-k_{ep}t} + v_p C_p(t), \quad (1)$$

where K^{trans} is the transfer rate constant, k_{ep} is the washout constant, v_p is the volume fraction of blood plasma, $\otimes$ represents convolution, $C_p(t)$ refers to the contrast concentration in the blood plasma and $C_t(t)$ refers to an individual concentration time curve. A separate parameter, v_e, represents the extracellular volume fraction and is equal to the quotient of K^{trans} and k_{ep} (derivation of this model and explanation of standardized parameters given in Ref. [32]).

Fitting the model given in Eq. (1) to the measured tissue concentration curves requires knowledge of the $C_p(t)$ time course, also known as the AIF. In this work, the AMM method was used to estimate the AIF directly from the simulated or measured tissue concentration curves [27]. Briefly, the AMM method takes a set of tissue concentration curves from a region of enhancing tissue in a DCE-MRI experiment and defines an objective function:

$$R = ||\overrightarrow{C_t(t)} - H\overrightarrow{C_p(t)}||, \quad (2)$$

where $C_t(t)$ is a matrix of N tissue activity curves, H is a Toeplitz matrix describing the discrete convolution in the ETK model and $C_p(t)$ is the AIF. This function is minimized by alternately refining the estimates for the model parameters

in H and the AIF estimate. A functional representation of the AIF, consisting of three gamma-variate curves and a sigmoid curve, is used to reduce the number of parameters to be estimated as well as to reduce the impact of measurement noise on the estimation.

2.3. Temporal resolution simulations

Computer simulations were done to assess the effect of temporal resolution on both the ETK and 3TP models. The increased spatial resolution possible with lower temporal sampling rates was not addressed in this study. We return to this point in the discussion. These simulations were based on previously acquired patient data. One hundred lesions were simulated according to the following strategy:

1. Kinetic parameters were determined voxelwise from DCE-MRI data from breast patients. Details of the acquisition are given below. The parameter values ranged from 0–2.5 min^{-1} for K^{trans}, 0–1.0 min^{-1} for k_{ep} and 0–0.28 for v_{p}.
2. A 'true' AIF was created by dispersing a population-averaged AIF with a Gaussian kernel. The width of the Gaussian kernel was a randomly selected value between 0 and 0.2 min. This dispersion was included so that the true AIF would not necessarily be equivalent to the population average, which was used to initialize the AMM algorithm described above. The dispersion used was consistent with AIFs measured in patients from a similar population as that described below. Sample dispersed AIFs can be seen in Fig. 1.
3. For each simulated lesion, 500 'true' tissue curves were created according to Eq. (1) using the 'true' AIF and the lesion kinetic parameters. Each set of 500 curves was generated with temporal resolutions of 1, 4, 8, 16, 32 and 64 s and 8-min simulated acquisition.
4. 'True' 3TP parameters were calculated for each of the tissue curves using the set of curves generated at 1-s resolution.
5. Zero-mean Gaussian noise with standard deviation of 0.03 mM was added independently to each true tissue curve at each temporal sampling rate. This noise level was the average noise level found in the lesions on which the simulations are based.
6. For each simulated lesion, at each temporal sampling rate, parameters were calculated using an AIF obtained from the AMM blind estimation method developed previously for use with the ETK model [27]. Prior to estimation, the noisy tissue curves were upsampled to 1-s resolution with cubic interpolation. The data were clustered into eight representative curves, as described in Ref. [27]. The AIF was estimated with 1-s resolution, and the kinetic parameters were calculated for each tissue curve with the upsampled AIF and tissue curves.
7. 3TP parameters were calculated for each tissue curve at each temporal sampling rate. The three time points were obtained by selecting a precontrast frame, and the time frames 2 min and 6 min post contrast injection. Colors and intensities for each curve were assigned as described above.

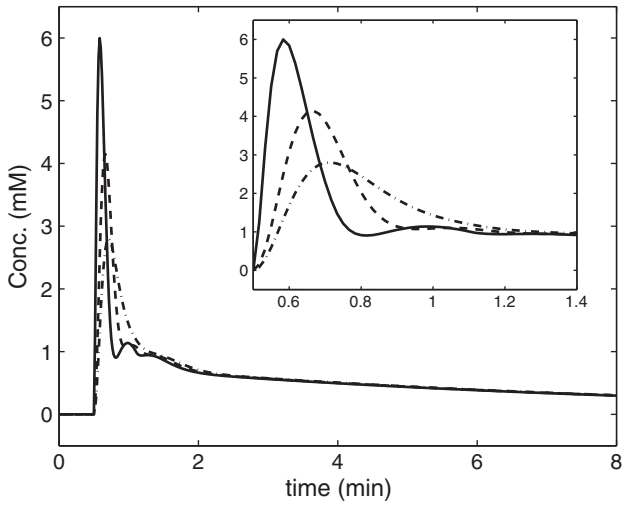

Fig. 1. Three sample AIFs used in the temporal resolution simulations. The first AIF (solid line) represents the population-average AIF. The dashed AIFs represent AIFs dispersed with kernels of width 0.1 and 0.2 min.

Fig. 2 displays representative tissue curves from the above simulations. Following the simulations, the root-mean-square error (RMSE) of the estimated parameters was calculated. For the ETK model errors, the RMSE was calculated based on the differences between the estimated parameters and the "true" parameter values on which the simulations were based. For the 3TP method, the errors were calculated based on the differences in intensity between the intensity values from the fully sampled curves and the temporally downsampled curves. For individual curves where the temporal downsampling resulted in classifying curves as a different color than the fully sampled curve, the intensity of the downsampled curve was set to zero. This was done as classification of tumors with the 3TP method is based on counting the number of voxels with a given color. The chosen method penalizes voxels that are miscolored after temporal downsampling. The errors were collected over all the simulated tumors, and average RMSE values for each temporal resolution were calculated.

2.4. Clinical data

The 3TP and ETK models were also applied to previously acquired breast DCE-MRI data from 87 patients. These data were collected as part of a prospective study of pharmacokinetic modeling in breast DCE [18]. All data were acquired on a 1.5-T Siemens Avanto scanner. The dynamic imaging was performed with 9.2–19.7-s temporal resolution using a fast three-dimensional Spoiled Gradient Echo sequence (repetition time/echo time/alpha=2.54/1.09/10) with 1.5-mm isotropic resolution. Twenty-four of the data sets had a

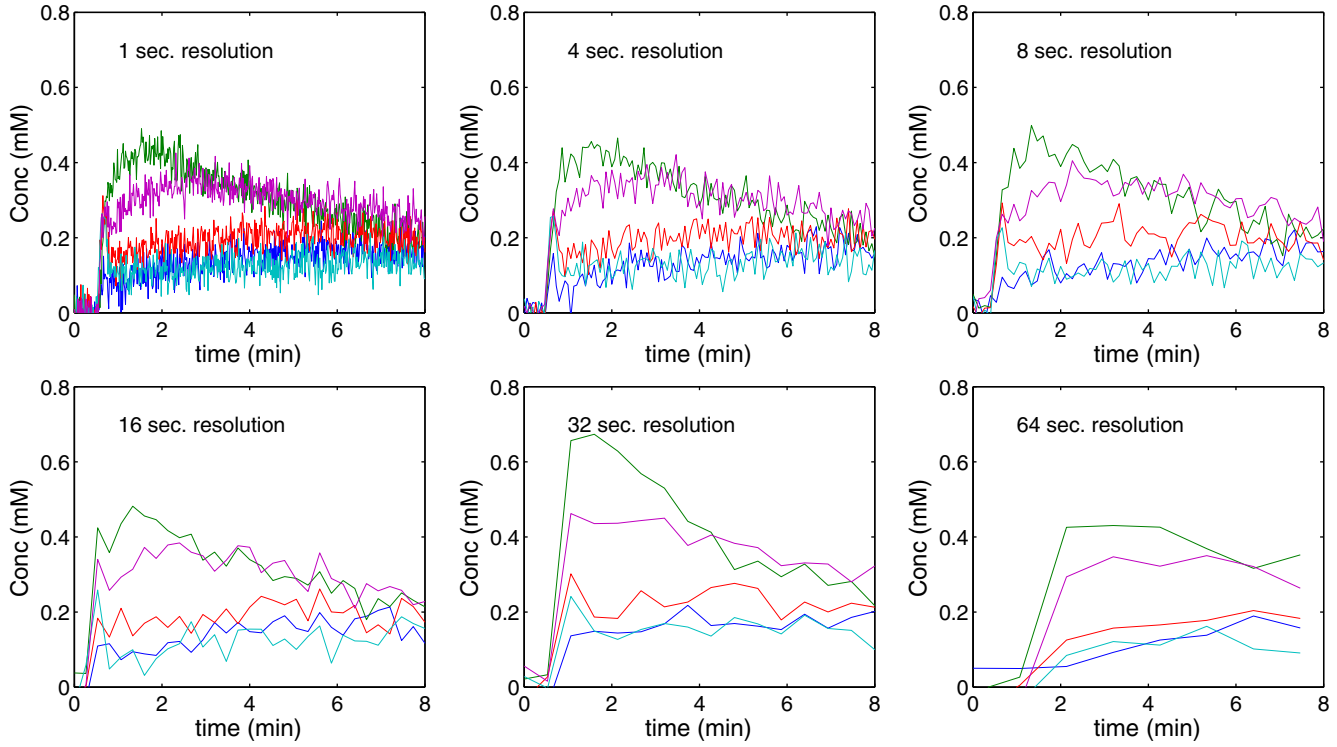

Fig. 2. Sample tissue curves from temporal resolution simulations. Each set of curves was created from kinetic parameters derived from previously acquired patient data. The tissue curves were created with 4-, 8-, 16-, 32- and 64-s temporal sampling, and Gaussian white noise (σ=0.03 mM) was added. True 3TP parameters were obtained from curves with 1-s resolution.

temporal resolution between 9.2 and 12 s. Forty-two of the data sets had temporal sampling rates between 12 and 16 s, and 21 of the data sets had a sampling rate between 16 and 19.7 s. Partial Fourier encoding in the phase and frequency encoding directions was used, and full bilateral coverage from the chest wall to the nipple was obtained in all scans. A 20-ml injection of gadodiamide (Omniscan, Amersham Health) was given at a rate of 4 ml/s, followed by a 20-ml saline flush at 2 ml/s. Eight to 10 min of data was acquired. Each of the data sets was downsampled temporally by a factor of 2 and 4. This downsampling was accomplished by selecting every second time frame and every fourth time frame to obtain data sets with temporal sampling rates ranging from 18.4 to 39.4 and 36.8 to 78.8 s/frame. We note that this method of downsampling is not actually identical to acquiring the data at different temporal resolutions. However, since performing multiple DCE-MRI acquisitions on each patient is not practical, the approach here serves as a useful approximation.

Each of the subjects in the previously referenced study had been referred to biopsy independent of any MRI results. All imaging results were correlated with pathology. In addition, following data acquisition, one region of interest (ROI) per patient was identified manually in each subject on

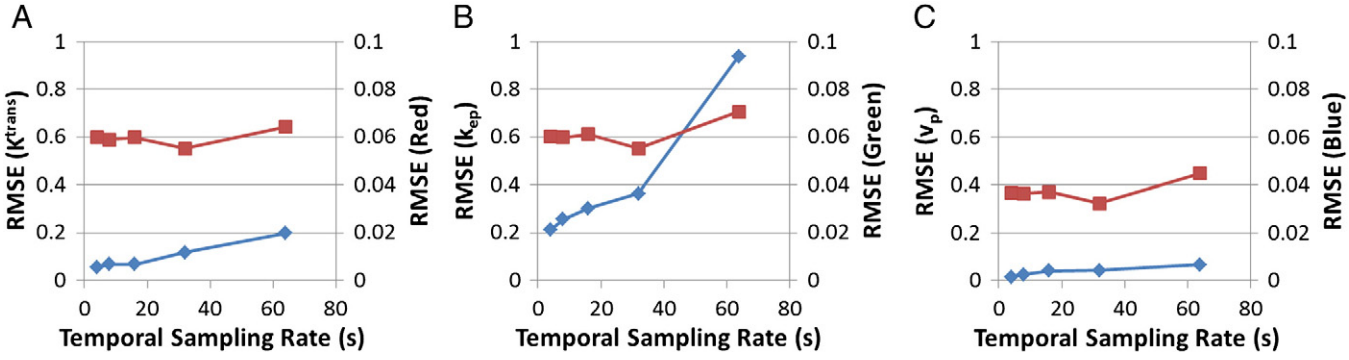

Fig. 3. The RMSE for each parameter for all of the temporal sampling simulations. Panel (A) corresponds to K^{trans}/red, (B) to k_{ep}/blue and (C) to v_p/red. In each panel, the green curve corresponds to ETK parameters with an AMM-estimated AIF, and the blue curve corresponds to 3TP parameters.

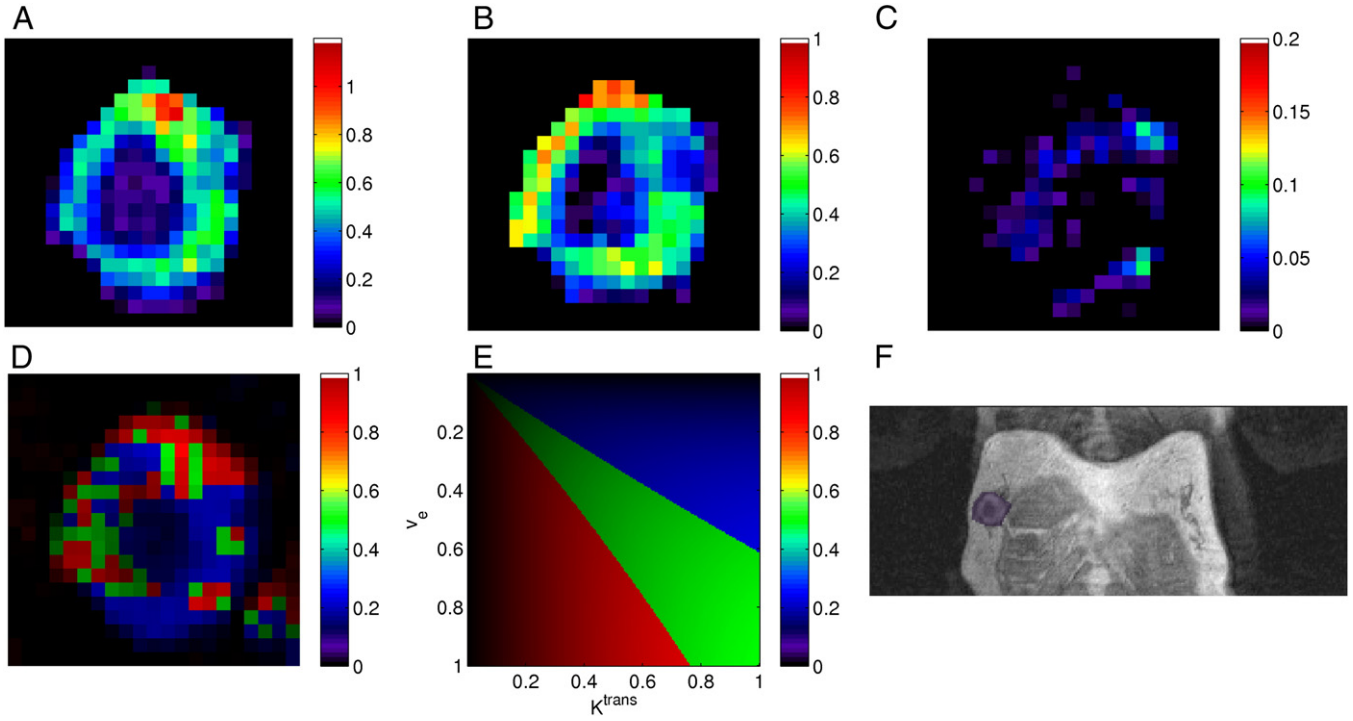

Fig. 4. Parameter maps from a representative slice of DCE-MRI data taken from the left breast of a patient with infiltrating ductal carcinoma. Panels (A–C) correspond to K^{trans}, k_{ep} and v_p values calculated with an AMM-estimated AIF and (D) to 3TP parameters. Panel (E) displays the calibration map used in the 3TP processing, and panel (F) displays a postcontrast T1-weighted axial slice highlighting the size and location of the lesion.

the postcontrast frames from the dynamic study by an experienced observer.

Pharmacokinetic parameters were calculated for each voxel within the defined ROIs. The AMM-estimated AIF was used, and separate calculations were done for both the original and two downsampled data sets. For the AMM method, all of the tissue curves within the ROI were used as input. These curves were clustered using an unsupervised k-means algorithm, and the cluster-averaged curves were used as input to the AMM algorithm. A population-average AIF, based on that reported by Parker et al. [23], was used to initialize the algorithm. Prior to estimation, the tissue curves were upsampled to 1-s resolution with cubic interpolation, and the AIF was estimated with a 1-s resolution sampling rate. This approach is similar to that used in the multiple reference tissue approach outline by Yang et al. [26] and was used to allow the AMM algorithm to estimate high-temporal-frequency aspects of the AIF. This AIF was then used to estimate kinetic parameters voxelwise throughout the field of view. Following parameter calculation, mean values for each of the parameters were found for each ROI. Parameters were also calculated for each voxel using the 3TP model described above.

Following parameter calculation, each of the lesions was classified as either benign or malignant. Classification of lesions with the 3TP parameters was done using the method outlined in Ref. [14], which distinguishes lesions based on the percentage of voxels assigned red. When a lesion has 15% or more red voxels, it is likely malignant. When the number of red voxels is less than 10%, the lesion is likely benign. For intermediate lesions, a second 3TP analysis with time points at 4 and 8 min after injection is done, and the lesion is reclassified.

For the ETK parameters, lesions were classified with linear combinations of parameters. Each of the possible linear combinations of parameters (i.e., K^{trans}, k_{ep}, v_p, K^{trans}/k_{ep}, K^{trans}/v_p, k_{ep}/v_p, $K^{trans}/k_{ep}/v_p$) was considered as a possible classifier. Parameters were combined using the method outlined in Ref. [18]. This method calculates the ROC curve for any pair of parameters p_1 and p_2 according to the linear combination $p=p_1\sin(\theta)-p_2\cos(\theta)$, where θ ranges from −180° to 180° in 1° increments. A similar method is used to extend the linear combination to three parameters. This was repeated for each patient in a leave-one-out manner with a possible unique classifier for each data set. A standard method [33] was used to calculate the ROC curves for each

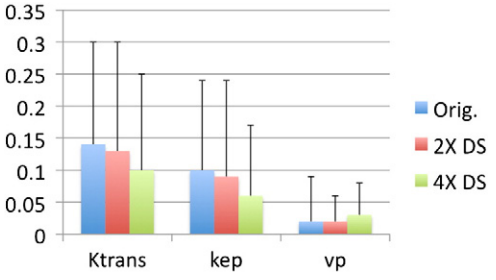

Fig. 5. Mean (+1 standard deviation) parameter values for the kinetic parameters of the clinical data studied at the originally sampled temporal resolution and after downsampling by a factor of 2 and 4. K^{trans} and k_{ep} are both measured in min^{-1}, while v_p is a fractional volume.

combination. Separate ROC curves were generated using the original data and each set of downsampled data.

Classification of the lesions for both the 3TP and ETK parameters was also done retrospectively to find the optimal linear combination of parameters that maximizes the AUC. As with the classification done for the ETK method above, each of the possible linear combinations of the parameters was tested (i.e., red, green, blue, red/green, red/blue, green/blue, red/green/blue). The intensities of the colors assigned to the voxels were used to classify the lesions. All of the lesions were included in the analysis, and the optimal linear classifier was found for both the 3TP and ETK parameters for each temporal resolution.

3. Results

3.1. Temporal resolution simulations

Aggregate results from all 100 simulated lesions are seen in Fig. 3. This figure displays the RMSE for the simulations at each temporal resolution for each parameter. The mean error in the ETK model with the AMM-estimated AIF increases nearly linearly with the temporal resolution of the input curves, from 0.06 to 0.20 for K^{trans}, from 0.21 to 0.94 for k_{ep} and from 0.02 to 0.07 for v_p. The RMSEs in the parameters from the 3TP method remained relatively constant as the temporal sampling changed as expected, changing by approximately 15% as the temporal sampling rate increased from 4 to 64 s. The errors in the 3TP parameters were largely due to incorrect binning of the voxels as the temporal resolution changed.

3.2. Clinical data

Fig. 4 displays modeling results from a representative slice from one of the lesions in this study. The first row shows the kinetic parameter values calculated with an AMM-estimated AIF. The second row displays the 3TP parameters for the same slice, along with the calibration map used for the 3TP parameters and a postcontrast T1-weighted image showing the tumor location within the body. These parameters were from a subject with pathology-proven infiltrating ductal carcinoma, and the elevated K^{trans} values seen here are consistent with literature reports [18]. The mean and standard deviations of these parameter values are seen in Fig. 5.

ROC curves for the 3TP method using a prospective classifier are plotted in Fig. 6. For each of the lesions used in this study, diagnoses were obtained from MRI-independent pathology reports. Of the lesions studied here, 25 were malignant including 16 invasive ductal carcinomas, 4 ductal carcinomas in situ, 2 atypical ductal hyperplasias, 1 atypical apocrine metaplasia, 1 atypical papilloma and 1 lobular carcinoma in situ. The remaining 62 lesions were benign. Using the classifier for the 3TP parameters, the AUC was 0.85, with a 95% confidence interval (CI) of 0.74–0.96. When the data were temporally downsampled by a factor of 2 prior to parameter calculation, the AUC of the ROC curve

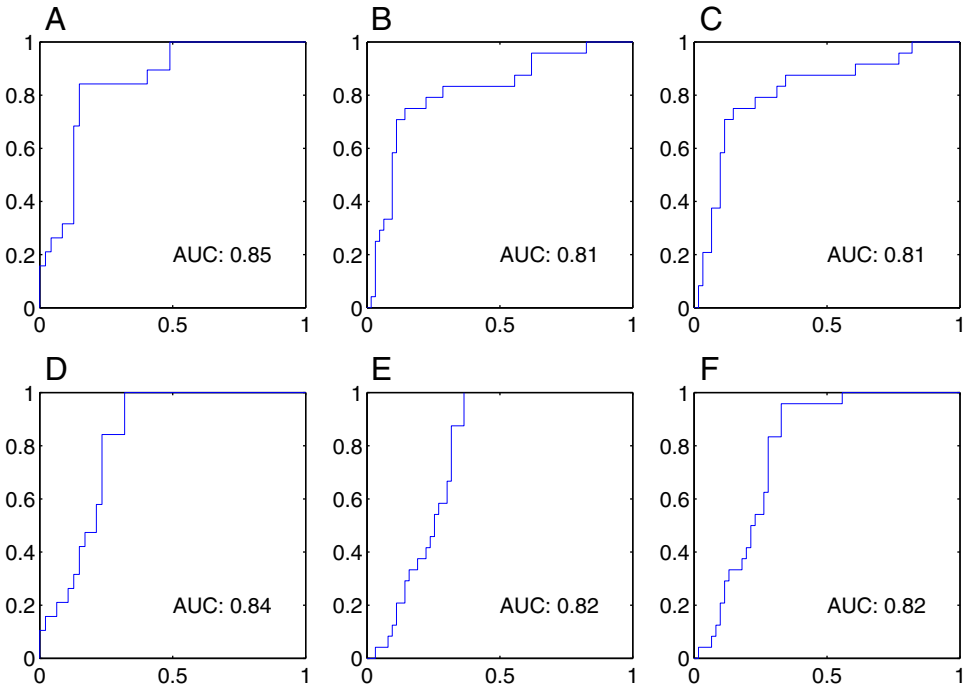

Fig. 6. ROC curves for the 3TP method using a literature (prospective) classifier as well as those for the ETK method using a leave-one-out analysis. The first row displays ROC curves for the 3TP method with the original data set (A), for the data downsampled by a factor of 2 (B) and for the data downsampled by a factor of 4 (C). The second row corresponds to the ETK method with the original data (D), as well as the downsampled data sets (E) and (F). The AUC is indicated on each plot.

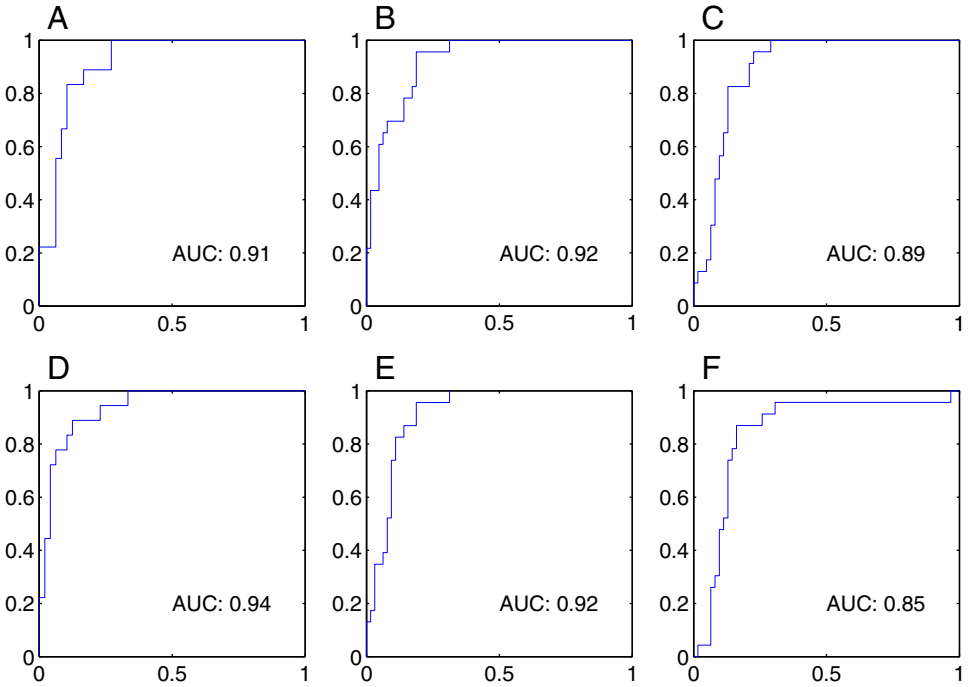

Fig. 7. ROC curves for both the 3TP and ETK methods using a retrospectively determined classifier. The first row displays ROC curves for the 3TP method with the original data set (A), for the data downsampled by a factor of 2 (B) and for the data downsampled by a factor of 4 (C). The second row corresponds to the ETK method with the original data (D), as well as the downsampled data sets (E) and (F). The AUC is indicated on each plot.

decreased to 0.81 (CI: 0.70–0.92). When the data were downsampled by a factor of 4, the 3TP classifier was unchanged, with an AUC of 0.81 (CI: 0.70–0.92). ROC curves for the ETK method are also shown in Fig. 6. These curves were generated using a leave-one-out analysis. At the native resolution of the scans, the AUC of the ROC curve was 0.85 (CI: 0.72–0.96). When the data were downsampled by a factor of 2, the AUC decreased to 0.82 (CI: 0.71–0.93). When the data were further downsampled, the AUC remained 0.82 (CI: 0.70–0.93).

When the optimal linear classifier was found retrospectively, the AUC for the 3TP increased. The ROC curves for both the 3TP and ETK methods with a retrospective classifier are seen in Fig. 7. The first row corresponds to values from the 3TP method, and the second row to the ETK analysis. For the original data set, with temporal sampling rates ranging from 9.2 to 19.7 s, the 3TP method AUC was 0.91 (CI: 0.82–1.00) and the ETK method AUC was 0.94 (CI: 0.86–1.00). The linear combinations of parameters that provided the highest AUC were 0.98red+0.21green for the 3TP model and $0.87K^{trans}+0.49k_{ep}$ for the ETK model. When the data were downsampled by a factor of 2, the 3TP AUC increased to 0.92 (CI: 0.85–1.00) and the ETK method decreased to 0.92 (CI: 0.84–0.99). The parameter combinations for these AUC values were 0.88red+0.47green for the 3TP model and $0.99K^{trans}-0.16k_{ep}$ for the ETK model. When the data were downsampled by a factor of 4, the 3TP AUC decreased to 0.89 (CI: 0.81–0.98) and the ETK method decreased to 0.85 (CI: 0.74–0.95). The parameter values for these AUC values were 0.14red+0.99green for the 3TP model and $0.88K^{trans}+0.47k_{ep}$ for the ETK model.

4. Discussion

This work presents results comparing the semiquantitative 3TP method and the fully quantitative ETK compartmental modeling method for evaluating breast DCE-MRI. Semiquantitative models, such as the 3TP method studied here, return parameters that are dependent on the overall shape of the tissue curves, and thus reflect tissue physiology only indirectly. As shown in the simulations carried out here, the accuracy of the 3TP method is insensitive to the temporal sampling rate of the acquired data. As a result, the analysis can be done with higher-spatial-resolution images in conjunction with morphological assessments [14]. In addition, the computational load of the 3TP method is minimal compared to the quantitative methods. In contrast, the parameters of the fully quantitative models, such as the ETK model studied here, directly reflect tissue physiology, though they require higher temporal resolution (with concomitant decreases in signal-to-noise ratio, or spatial resolution) to be accurately measured.

In this work, the AIF was estimated with the AMM algorithm. Estimating the input function allows for greater interpatient individuality than a population-average input function. The estimation can be done on grids with an arbitrarily high temporal sampling rate, allowing for estimation of higher-frequency components in the AIF than would be

available at lower sampling rates. In practice, 1-s temporal sampling rates may be impractical in clinical settings. Technical limitations on the data acquisition, as well as the need for high spatial resolution, restrict the rate at which data can be acquired. New developments in image acquisition and reconstruction may alleviate these concerns. A second limitation is the underlying relaxation times of the tissue. In a standard DCE-MRI acquisition, the magnetization of the tissue must be allowed to relax back to a steady state between readouts. If the tissue is not at a steady state, the acquired signal will be inconsistent between acquisitions, which will lead to interpretation errors.

Despite the high-resolution sampling rate that can be used for the AIF estimation, the information available from the tissue curves will depend on the native sampling rate. Henderson et al. report that for curves with nonzero contribution from the blood plasma volume (v_p) and with a known AIF, the tissue curves must be sampled with at least 4-s resolution to obtain less then 10% error in all of the parameter estimates [29]. This same study reports that if errors in the plasma volume are ignored, the sampling rate can be relaxed to 16 s to obtain less than 10% error in the K^{trans} and k_{ep} estimates. In a similar study, Schabel et al. report results from simulations on the effects of changing the temporal sampling rate on the accuracy of kinetic parameters. This work was done with a blind Monte-Carlo-type estimation method for obtaining the AIF. This type of blind AIF estimation method can be considered a generalization of the AMM method employed here [28]. The simulations carried out by Schabel et al. return good estimates of all the parameters at reasonable noise levels and at sampling rates up to 8 s, after which the errors grow rapidly with increasing sampling rates. The blind Monte Carlo method also found that, ignoring any errors in v_p, K^{trans} and k_{ep} estimates were stable up to sampling rates of 12 s, after which the error increased rapidly. In contrast, work with the reference region model, which does not explicitly define an AIF and which ignores any contributions from the blood plasma volume, has shown that temporal sampling rates can increase up to 60 s with little bias in K^{trans} or k_{ep} [17,30,31]. This may be due to the relatively dispersed AIF used to evaluate this method. A slower simulated injection with a longer temporal footprint will relax the sampling requirements on the resultant tissue curves. The amount of dispersion between the AIF as measured in the aorta and that actually seen by the breast tissue remains an open question.

The fastest sampling in the clinical data studied here was more than twice as long as the 4 s recommended by Henderson et al. and more than 1 s faster than the 8 s reported by Schabel et al. As a result, voxels with nonzero v_p are not sampled sufficiently quickly, and much of that information is lost, even with a high-resolution sampling rate for AIF estimation. In lesions where v_p is small enough to be neglected, the recommendation of Henderson et al. for the required sampling rate increases to 16 s [29], while the recommendation of Schabel et al. increases only to 12 s [28]. In comparison, the temporal sampling rate of the data acquired here ranges up to 19.7 s. More work is needed to understand the relationship between nonzero v_p and the AIF estimation at nonoptimal temporal sampling rates.

One shortcoming in this study is the lack of an absolute reference with which to compare the parameters estimated by each of the tested methods. In this work, we measure the usefulness of a method by its ability to distinguish lesions as malignant or benign. One potential shortcoming of this study is that the selection of an optimal linear classifier based on the analysis parameters remains an open question for both quantitative and semiquantitative analysis. As seen in Fig. 6, the literature classifier used in conjunction with the 3TP method yields good results (AUC>0.8) regardless of the temporal resolution and is comparable to similar studies with other semiquantitative analysis methods [34]. As mentioned in Ref. [14], this classifier is often used in conjunction with radiologist interpretation of the images to arrive at a diagnosis. The leave-one-out method returned similar results using the ETK parameters, which suggest that a prospective classifier based on the ETK model may be clinically feasible at the temporal sampling rates studied here for discrimination between benign and malignant tumors. Regardless of the temporal sampling rate, in some voxels, the ETK model will not be able to fit the measured data exactly, which could result in additional errors in tissue classification.

A second potential limitation of this work is the approach used to downsample the clinically acquired data. Recent work by Heisen et al. [31] utilizes a k-space-based downsampling strategy that more accurately reflects the effects of changing the temporal sampling rate on the acquired images. In this work, the k-space data were not available for each patient, and utilizing this downsampling strategy was not possible for the clinical data. In contrast, the simulations carried out here generate tissue curves with given input functions and tissue parameters at various temporal sampling rates, which avoid the problems that may arise from various downsampling techniques.

As with previous analyses of various diagnostic techniques [18,34], the pathology-proven diagnoses allowed the selection of a retrospectively determined classifier for optimally distinguishing benign and malignant lesions. This was especially useful for the ETK analysis, where no consensus has been reached on how to classify lesions based on the estimated parameters. As seen in Fig. 7, the optimal linear 3TP classifier outperforms the literature classifier for the 3TP method. The increase in the AUC is due to the large number of parameter combinations tested when finding the optimal retrospective linear classifier. This type of retrospective analysis is not typically used in conjunction with the 3TP parameters, but is included here to allow for direct comparison with the ETK method. For the 3TP method, the change in the optimal classifier performance, as measured by the AUC, is small as the temporal resolution of the data lengthens. This is due to the general insensitivity of the 3TP method to temporal sampling within the range of this study.

The ETK method, on the other hand, is more sensitive to the temporal sampling of the acquired data. For the most rapidly sampled data, the ETK method had the highest overall optimal performance. As the temporal sampling rate increased, the AUC of the ROC curves for the ETK method decreased more rapidly than that for the 3TP method.

Another limitation of this study is that the analysis performed here did not include any morphological assessment of the acquired data. The increased temporal sampling rate of the data used in this study led to a decrease in the acquired spatial resolution (1.5-mm isotropic resolution here, compared to submillimeter resolution obtained in more standard breast DCE-MRI scans). Morphological assessment, when combined with the semiquantitative or quantitative analyses studied here, may provide additional power in distinguishing lesions, though the extent of the additional distinguishing power is left to future studies. Future work will focus on the combined effects of spatial and temporal resolution on the distinguishing power of the ETK or 3TP method.

5. Conclusion

In this work, we studied the effect of changing the temporal sampling rate on two different analysis methods for evaluating DCE-MRI data in breast cancer. The error in the parameters for ETK model was shown in simulation to increase approximately linearly as the temporal sampling rate increased from 4 to 64 s per frame. The error in the parameters from the 3TP method remained relatively constant in simulation over the same range. When applied to clinical data acquired at 9–19-s/frame temporal resolution, the ETK analysis was able to distinguish benign and malignant lesions more accurately than the 3TP analysis when optimally determined classifiers were used as determined by the AUC. As the data were increasingly undersampled temporally, the ETK performance decreased to a level equal to that of the 3TP analysis. With further temporal undersampling, the ETK method's performance was worse than that for the 3TP method. As most current clinical scans involve acquisitions of 1 min per time frame, use of the ETK method with such data sets may not provide any benefit over the 3TP method for the task of discriminating between benign and malignant tumors. As undersampling acquisition and reconstruction techniques improve, high-temporal-resolution acquisition of DCE-MRI data without any loss in spatial resolution will become more realizable. The ability of the fully quantitative modeling to report on subject physiology may make it a more attractive analysis option than semiquantitative analyses, especially with no expected loss in distinguishing power relative to semiquantitative analyses.

References

[1] Lord SJ, Lei W, Craft P, Cawson JN, Morris I, Walleser S, et al. A systematic review of the effectiveness of magnetic resonance imaging (MRI) as an addition to mammography and ultrasound in screening young women at high risk of breast cancer. Eur J Cancer 2007;43(13):1905–17.

[2] Turnbull LW. Dynamic contrast-enhanced MRI in the diagnosis and management of breast cancer. NMR Biomed 2009;22(1):28–39.

[3] Chou CP, Wu MT, Chang HT, Lo YS, Pan HB, Degani H, et al. Monitoring breast cancer response to neoadjuvant systemic chemotherapy using parametric contrast-enhanced MRI: a pilot study. Acad Radiol 2007;14(5):561–73.

[4] Martincich L, Montemurro F, De Rosa G, Marra V, Ponzone R, Cirillo S, et al. Monitoring response to primary chemotherapy in breast cancer using dynamic contrast-enhanced magnetic resonance imaging. Breast Cancer Res Treat 2004;83(1):67–76.

[5] Chen W, Giger ML, Bick U, Newstead GM. Automatic identification and classification of characteristic kinetic curves of breast lesions on DCE-MRI. Med Phys 2006;33(8):2878–87.

[6] Eyal E, Badikhi D, Furman-Haran E, Kelcz F, Kirshenbaum KJ, Degani H. Principal component analysis of breast DCE-MRI adjusted with a model-based method. J Magn Reson Imaging 2009;30(5):989–98.

[7] Agner SC, Soman S, Libfeld E, McDonald M, Thomas K, Englander S, et al. Textural kinetics: a novel dynamic contrast-enhanced (DCE)-MRI feature for breast lesion classification. J Digit Imaging 2010.

[8] Degani H, Gusis V, Weinstein D, Fields S, Strano S. Mapping pathophysiological features of breast tumors by MRI at high spatial resolution. Nat Med 1997;3(7):780–2.

[9] Furman-Haran E, Grobgeld D, Kelcz F, Degani H. Critical role of spatial resolution in dynamic contrast-enhanced breast MRI. J Magn Reson Imaging 2001;13(6):862–7.

[10] Weinstein D, Strano S, Cohen P, Fields S, Gomori JM, Degani H. Breast fibroadenoma: mapping of pathophysiologic features with three-time-point, contrast-enhanced MR imaging — pilot study. Radiology 1999;210(1):233–40.

[11] Furman-Haran E, Degani H. Parametric analysis of breast MRI. J Comput Assist Tomogr 2002;26(3):376–86.

[12] Furman-Haran E, Grobgeld D, Margalit R, Degani H. Response of MCF7 human breast cancer to tamoxifen: evaluation by the three-time-point, contrast-enhanced magnetic resonance imaging method. Clin Cancer Res 1998;4(10):2299–304.

[13] Hauth EA, Stockamp C, Maderwald S, Muhler A, Kimmig R, Jaeger H, et al. Evaluation of the three-time-point method for diagnosis of breast lesions in contrast-enhanced MR mammography. Clin Imaging 2006;30(3):160–5.

[14] Kelcz F, Furman-Haran E, Grobgeld D, Degani H. Clinical testing of high-spatial-resolution parametric contrast-enhanced MR imaging of the breast. AJR Am J Roentgenol 2002;179(6):1485–92.

[15] Eyal E, Degani H. Model-based and model-free parametric analysis of breast dynamic-contrast-enhanced MRI. NMR Biomed 2009;22(1):40–53.

[16] Li KL, Henry RG, Wilmes LJ, Gibbs J, Zhu X, Lu Y, et al. Kinetic assessment of breast tumors using high spatial resolution signal enhancement ratio (SER) imaging. Magn Reson Med 2007;58(3):572–81.

[17] Planey CR, Welch EB, Xu L, Chakravarthy AB, Gatenby JC, Freehardt D, et al. Temporal sampling requirements for reference region modeling of DCE-MRI data in human breast cancer. J Magn Reson Imaging 2009;30(1):121–34.

[18] Schabel MC, Morrell GR, Oh KY, Walczak CA, Barlow RB, Neumayer LA. Pharmacokinetic mapping for lesion classification in dynamic breast MRI. J Magn Reson Imaging 2010;31(6):1371–8.

[19] Chen J, Yao J, Thomasson D. Automatic determination of arterial input function for dynamic contrast enhanced MRI in tumor assessment. Med Image Comput Comput Assist Interv 2008;11(Pt 1):594–601.

[20] Kjolby BF, Mikkelsen IK, Pedersen M, Ostergaard L, Kiselev VG. Analysis of partial volume effects on arterial input functions using gradient echo: a simulation study. Magn Reson Med 2009;61(6):1300–9.

[21] Fluckiger JU, Schabel MC, DiBella EV. Towards local arterial input functions in dynamic contrast-enhanced MRI. J Magn Reson Imaging 2010.

[22] Schabel MC, DiBella EV, Jensen RL, Salzman KL. A model-constrained Monte Carlo method for blind arterial input function estimation in dynamic contrast-enhanced MRI: II. In vivo results. Phys Med Biol 2010;55(16):4807–23.

[23] Parker GJ, Roberts C, Macdonald A, Buonaccorsi GA, Cheung S, Buckley DL, et al. Experimentally-derived functional form for a population-averaged high-temporal-resolution arterial input function for dynamic contrast-enhanced MRI. Magn Reson Med 2006;56(5): 993–1000.

[24] Yankeelov TE, Cron GO, Addison CL, Wallace JC, Wilkins RC, Pappas BA, et al. Comparison of a reference region model with direct measurement of an AIF in the analysis of DCE-MRI data. Magn Reson Med 2007;57(2):353–61.

[25] Yankeelov TE, Luci JJ, Lepage M, Li R, Debusk L, Lin PC, et al. Quantitative pharmacokinetic analysis of DCE-MRI data without an arterial input function: a reference region model. Magn Reson Imaging 2005;23(4):519–29.

[26] Yang C, Karczmar GS, Medved M, Stadler WM. Multiple reference tissue method for contrast agent arterial input function estimation. Magn Reson Med 2007;58(6):1266–75.

[27] Fluckiger JU, Schabel MC, DiBella EV. Model-based blind estimation of kinetic parameters in dynamic contrast enhanced (DCE)-MRI. Magn Reson Med 2009:1477–86.

[28] Schabel MC, Fluckiger JU, DiBella EV. A model-constrained Monte Carlo method for blind arterial input function estimation in dynamic contrast-enhanced MRI: I. Simulations. Phys Med Biol 2010;55(16): 4783–806.

[29] Henderson E, Rutt BK, Lee TY. Temporal sampling requirements for the tracer kinetics modeling of breast disease. Magn Reson Imaging 1998;16(9):1057–73.

[30] Heisen M, Fan X, Buurman J, van Riel NA, Karczmar GS, ter Haar Romeny BM. The use of a reference tissue arterial input function with low-temporal-resolution DCE-MRI data. Phys Med Biol 2010;55(16): 4871–83.

[31] Heisen M, Fan X, Buurman J, van Riel NA, Karczmar GS, ter Haar Romeny BM. The influence of temporal resolution in determining pharmacokinetic parameters from DCE-MRI data. Magn Reson Med 2010;63(3):811–6.

[32] Tofts PS, Brix G, Buckley DL, Evelhoch JL, Henderson E, Knopp MV, et al. Estimating kinetic parameters from dynamic contrast-enhanced T(1)-weighted MRI of a diffusable tracer: standardized quantities and symbols. J Magn Reson Imaging 1999;10(3): 223–32.

[33] Fawcett T. ROC Graphs: notes and practical considerations for researchers. HP Labs Tech Rep 2003.

[34] El Khouli RH, Macura KJ, Barker PB, Habba MR, Jacobs MA, Bluemke DA. Relationship of temporal resolution to diagnostic performance for dynamic contrast enhanced MRI of the breast. J Magn Reson Imaging 2009;30(5):999–1004.